SUPPORTING INFORMATION

Mainstream partial nitritation and anammox: long-term process stability and effluent quality at low temperatures

Michele Laureni[1,2,*], Per Falås[1], Orlane Robin[1,3], Arne Wick[4], David G. Weissbrodt[1,2,5,6], Jeppe Lund Nielsen[6], Thomas A. Ternes[4], Eberhard Morgenroth[1,2], Adriano Joss[1]

[1] Eawag: Swiss Federal Institute of Aquatic Science and Technology, Überlandstr. 133, 8600 Dübendorf, Switzerland

[2] Institute of Environmental Engineering, ETH Zürich, Stefano-Franscini-Platz 5, CH-8093 Zürich, Switzerland

[3] Institut National Polytechnique de Toulouse (INPT) - Ecole Nationale Supérieure des Ingénieurs en Arts Chimiques et Technologiques (ENSIACET), 4 allée Emile Monso, CS 44362, 31030 Toulouse cedex 4, France

[4] Federal Institute of Hydrology, Am Mainzer Tor 1, D-56068 Koblenz, Germany

[5] Department of Biotechnology, Delft University of Technology, Julianalaan 67, NL-2628 BC Delft, The Netherlands

[6] Department of Chemistry and Bioscience, Aalborg University, Fredrik Bajers Vej 7H, DK-9220 Aalborg, Denmark

*Corresponding author: Michele Laureni (michele.laureni@eawag.ch)

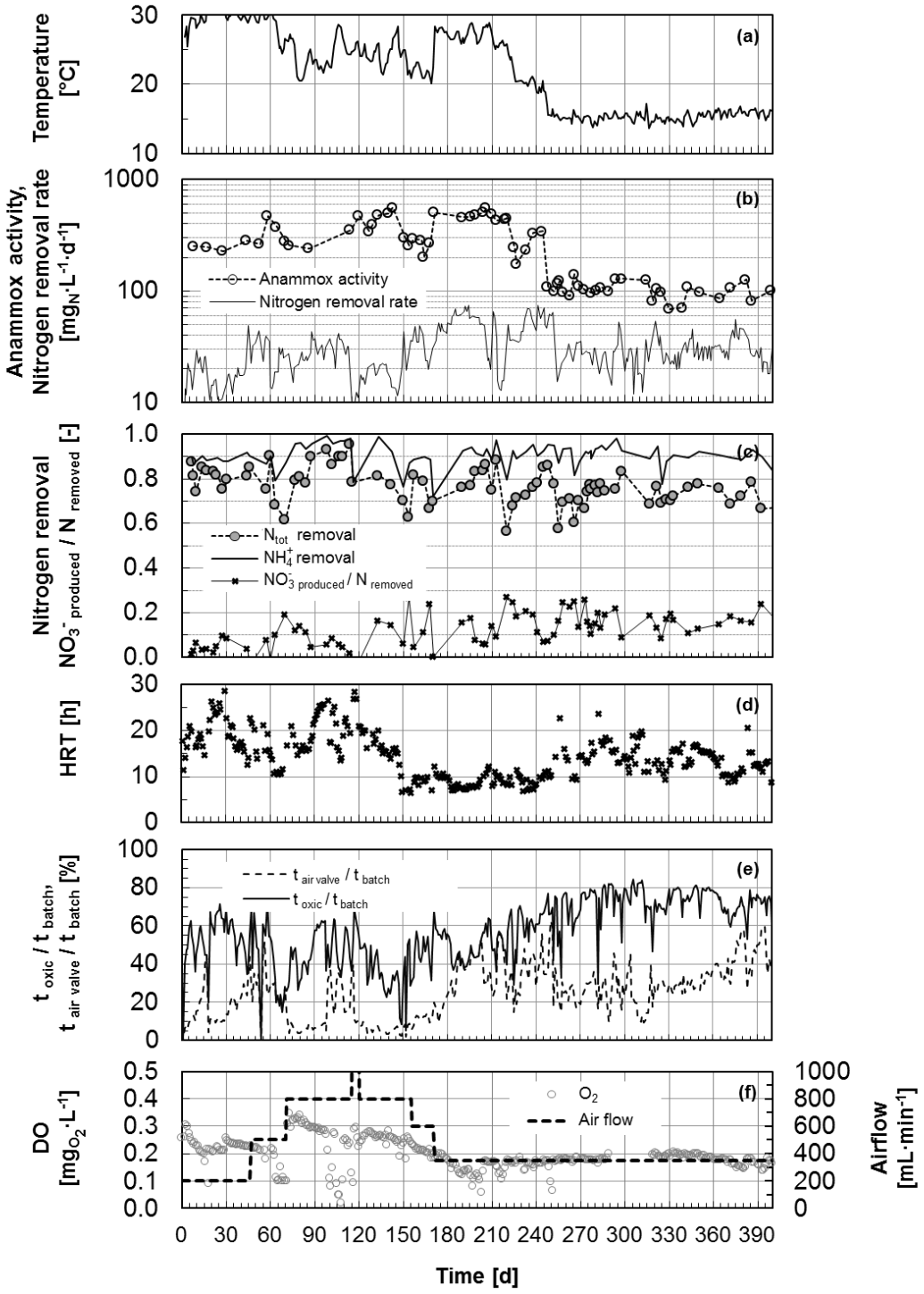

Figure S1 Conditions and performance of the MBBR during the whole operational period. Time series of temperature (a); maximum anammox activity ($mg_{(NH4+NO2)-N}·L^{-1}·d^{-1}$) and overall total nitrogen removal rate ($mg_N·L^{-1}·d^{-1}$) (b); total and ammonium nitrogen removals, and yield of NO_3^- production over total nitrogen removed (c); hydraulic retention time (HRT) (d); oxic time over total batch time (t_{oxic}/t_{batch}) and time the air valve was open, depending on airflow, over total batch time ($t_{air\ valve}/t_{batch}$) (e); average dissolved oxygen (DO) concentration during oxic time and airflow (f).

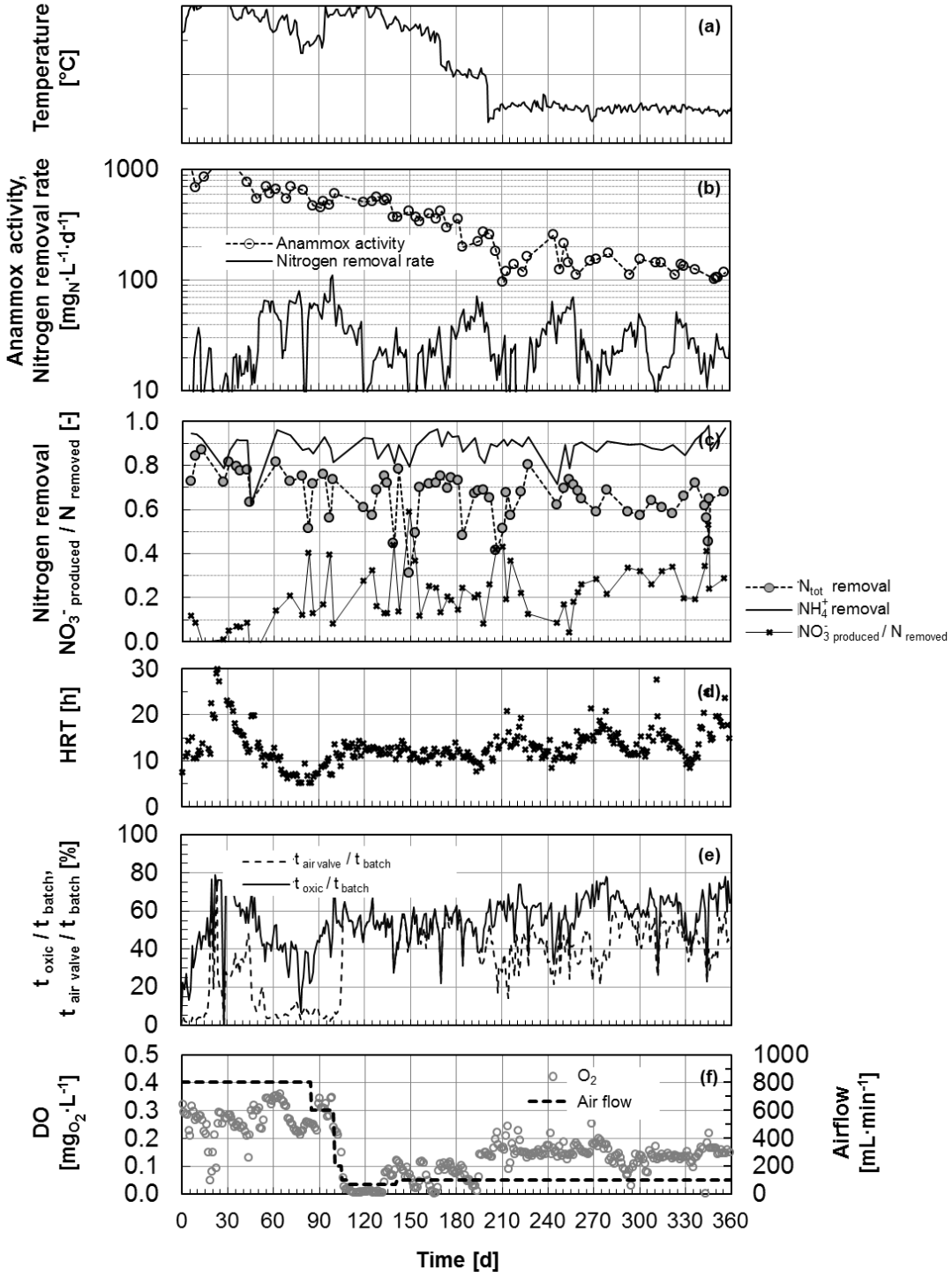

Figure S2 Conditions and performance of the H-MBBR during the whole operational period. Time series of temperature (a); maximum anammox activity ($mg_{(NH4+NO2)-N}·L^{-1}·d^{-1}$) and overall total nitrogen removal rate ($mg_N·L^{-1}·d^{-1}$) (b); total and ammonium nitrogen removals, and yield of NO_3^- production over total nitrogen removed (c); hydraulic retention time (HRT) (d); oxic time over total batch time (t_{oxic}/t_{batch}) and time the air valve was open, depending on airflow, over total batch time ($t_{air\ valve}/t_{batch}$) (e); average dissolved oxygen (DO) concentration during oxic time and airflow (f).

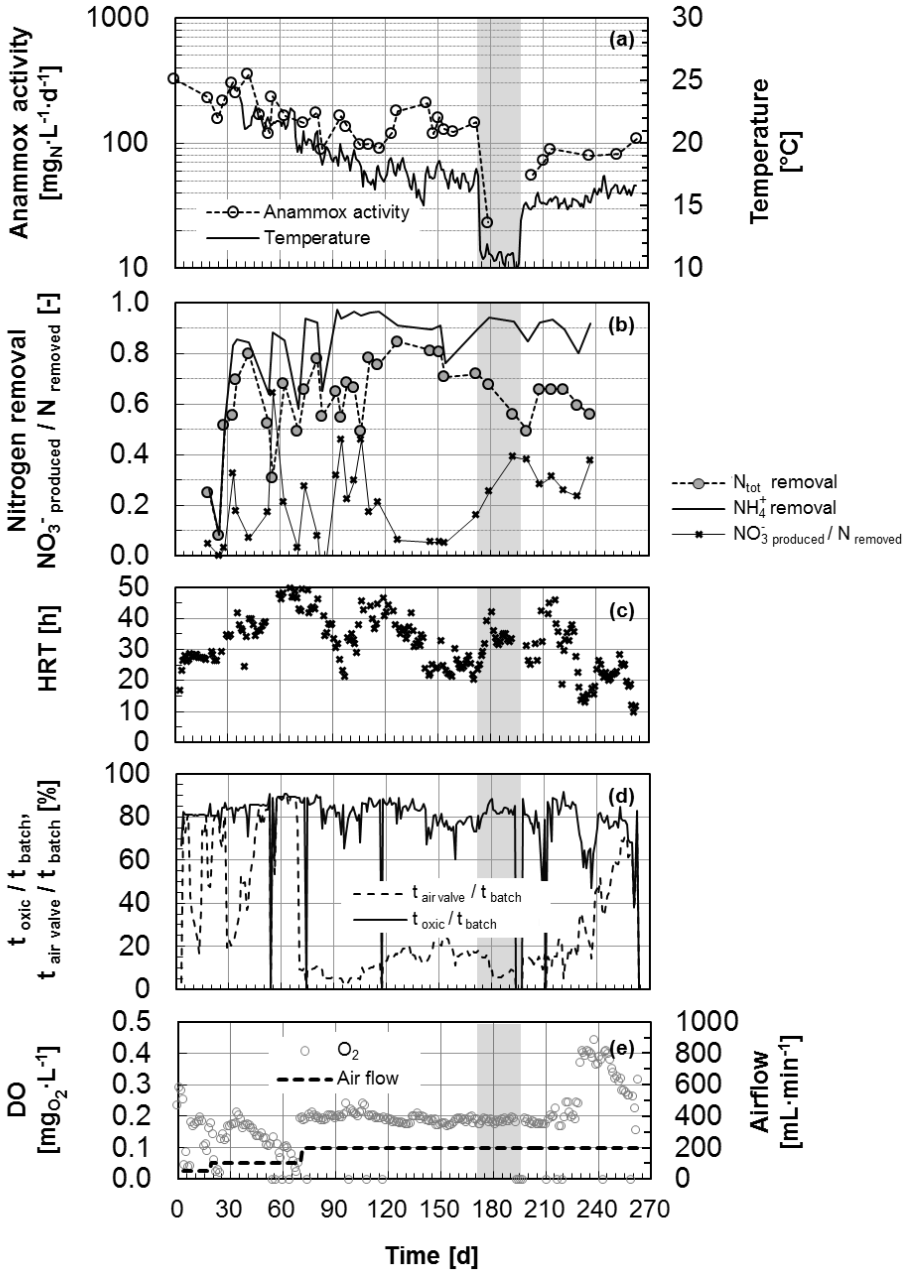

Figure S3 Conditions and performance of the MBBR-2 during the whole operational period. Time series of temperature and maximum anammox activity ($mg_{(NH4+NO2)-N}·L^{-1}·d^{-1}$) (a); total and ammonium nitrogen removals, and yield of NO_3^- production over total nitrogen removed (b); hydraulic retention time (HRT) (c); oxic time over total batch time (t_{oxic}/t_{batch}) and time the air valve was open, depending on airflow, over total batch time ($t_{air\ valve}/t_{batch}$) (d); average dissolved oxygen (DO) concentration during oxic time and airflow (e).

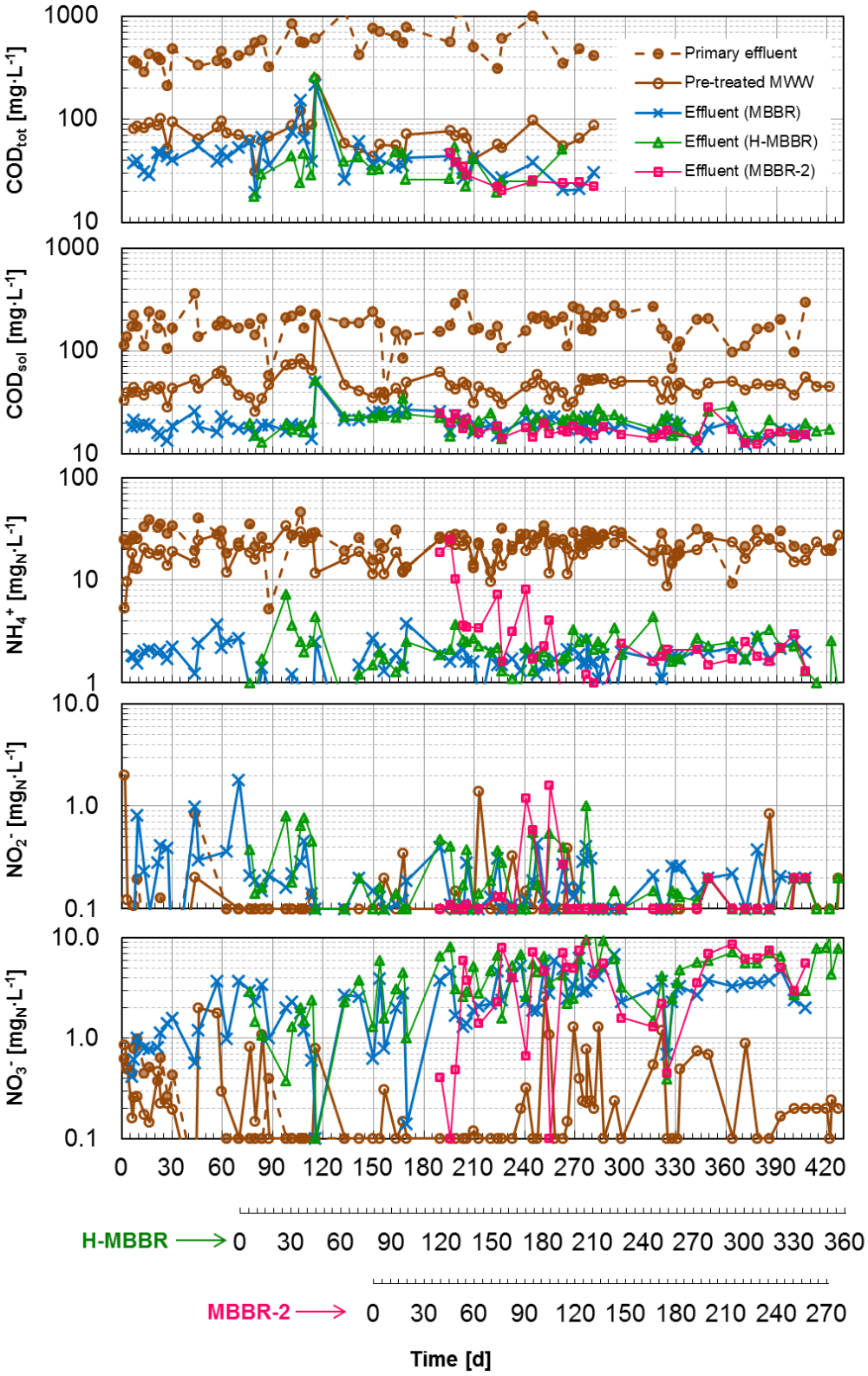

Figure S4 Time evolution of the concentrations of the total (COD_{tot}) and dissolved organic matter (COD_{sol}) and of the nitrogen species (NH_4^+, NO_2^-, NO_3^-) in the primary effluent, pre-treated MWW and effluents during the whole operational period. Note that due to different inoculation times, the values of MBBR (×), H-MBBR (▲) and MBBR-2 (■) effluent refer to a different time axis.

S5 Details of LC-MS/MS analysis

Chromatographic separation was achieved using a Zorbax Eclipse Plus C-18 column (2.1 x 150 mm, 3.5 mm, Agilent Technologies, Waldbronn, Germany). Ultrapure water and methanol (both supplemented with 0.1% formic acid) served as mobile phase A and B. The gradient elution applied was as follows: 100% A for 1 min, decrease to 80% A within 1 min, further decrease to 0% A within 14.5 min, hold isocratic at 0% A for 5.5 min, increase to initial conditions (100% A) within 0.1 min and hold isocratic for 6 min. The total runtime was 28 min and the flowrate and column temperature were set to 0.3 mL/min and 30°C respectively.

All target compounds were measured within one chromatographic run by scheduled multiple reaction monitoring (sMRM) using electrospray ionization (ESI) in both negative and positive mode. For polarity switching the settling time was set to 50 ms. The sMRM parameters were set as follows: detection window, 80 s; target scan time, 0.2 s; pause time, 3 ms. At least two mass transitions were measured for quantification and confirmation.

The limit of quantification (LOQ) was derived from the signal-to-noise (S/N) ratio in the native samples. At the LOQ, the S/N ratio of the mass transitions used for quantification and confirmation had to be at least 10 and 3 respectively. An internal standard calibration was used for quantification. The accuracy and precision of the method was checked within each measurement series by recovery experiments (spiking level 1 µg/L, $n \geq 3$) and repeated injections of reference samples. The results were only considered valid if the recovery was in the range of 75-125%.

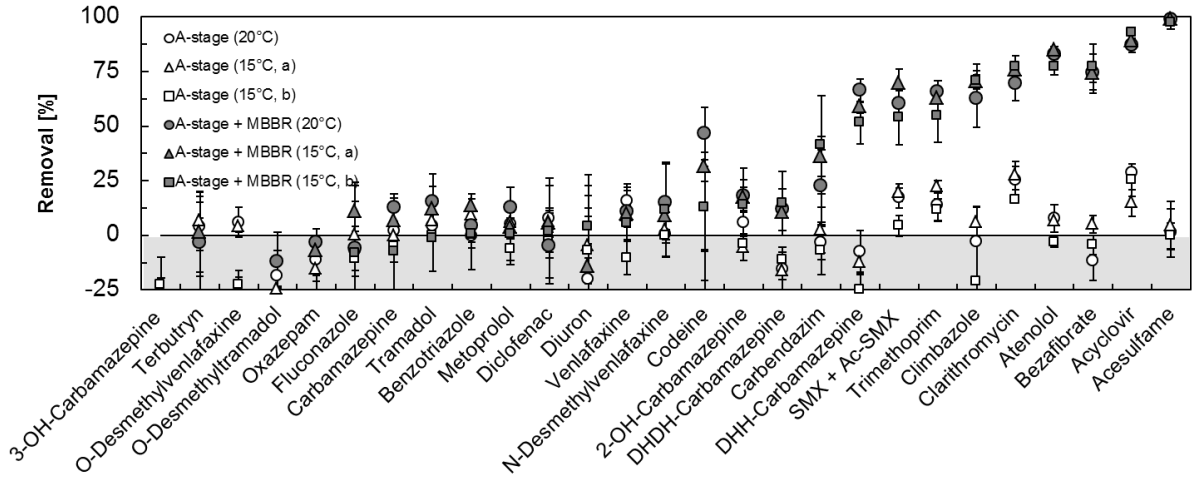

Figure S5 Removal of the studied organic micropollutants in the treatment scheme comprising the A-stage followed by the MBBR PN/A system. Comparison between the three subsequent sampling campaigns, days 239-244 (20°C), days 273-280 (15°C, a) and days 326-333 (15°C, b). *A-stage*: pre-treatment for COD removal only; *A-stage+MBBR:* full treatment scheme. The concentrations detected in the MWW served as the initial concentration C_0 for calculation of the removal (C/C_0) in the different systems. Compounds displaying removals in the range 0±25% are here considered as persistent. Error bars display standard deviations of 48-h composite samples (n=3). Micropollutants acronyms: DHH- Carbamazepine : 10,11-dihydro-10-hydroxy-carbamazepine; DHDH-Carbamazepine: 10,11-dihydro-10,11-dihydroxy-carbamazepine; SMX + Ac-SMX: sum of sulfamethoxazole and N_4-acetylsulfamethoxazole.

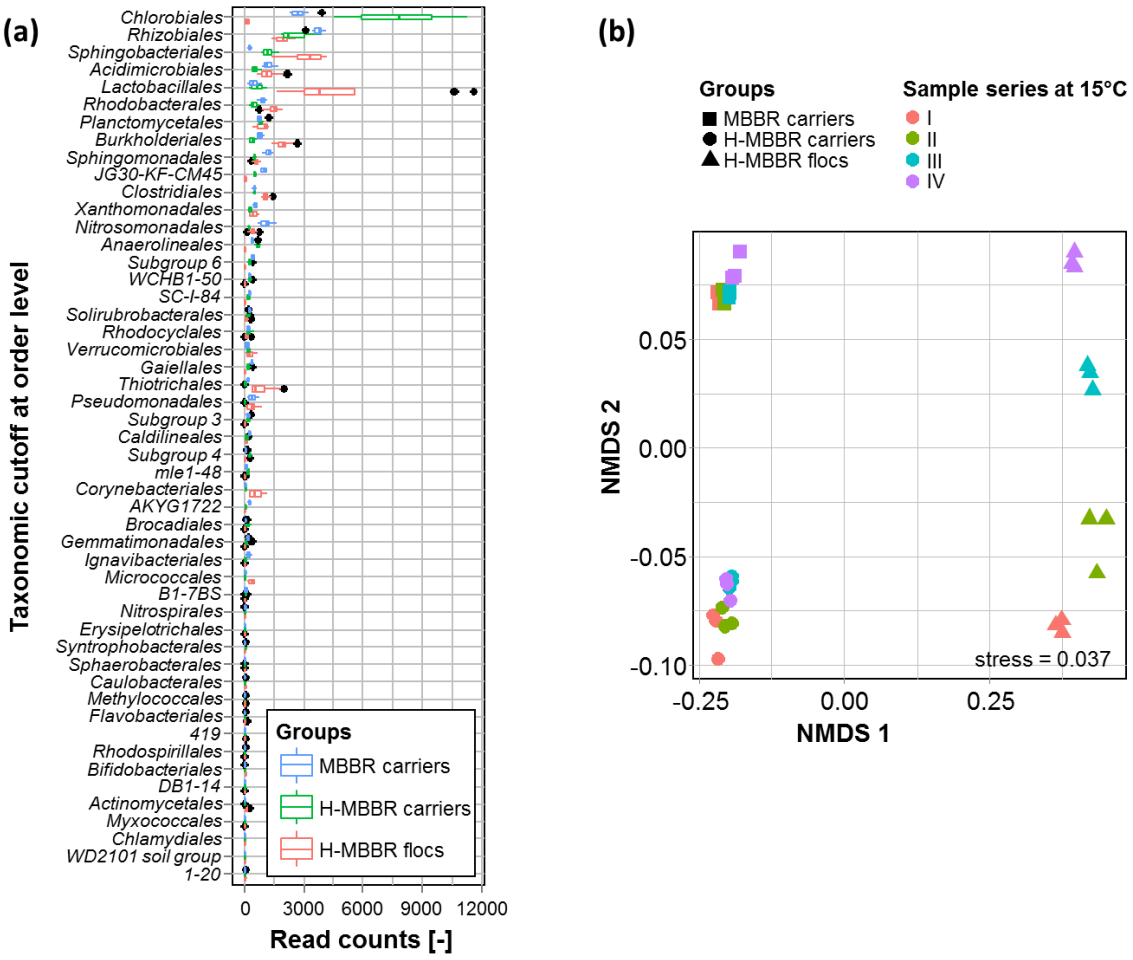

Figure S6 Comparison of bacterial community structures of the MBBR (solely biofilm carriers) and H-MBBR (biofilm carriers and floc fraction) collected along four time points (I: days 249 and 219; II: days 290 and 255; III: days 326 and 295; IV: days 390 and 350 respectively) during operation at 15°C and analyzed in triplicates via 16S rRNA gene-based amplicon sequencing targeting the v4 hypervariable region. Rank-ordered box plot of the 50 predominant bacterial orders detected in the three different types of biomass over the total sampling period at 15°C (a). Comparison of the bacterial community structures of the three different types of biomass discretized over the four sampling times by non-metric multidimensional scaling (NMDS) (b). The bacterial communities of the attached biomasses of the MBBR and H-MBBR displayed greater similarity over the respective four time points (displayed by compact groups) than the floc fraction of the H-MBBR (temporal dispersion along the second NMDS axis). The stress factor of 0.037 indicates high goodness of fit for the multidimensional regressions. The sequencing datasets were mapped and processed using the MiDAS field guide to the microbes of activated sludge (McIlroy *et al.* 2015).

Table S1 Stoichiometric matrix used for the estimation of the actual volumetric activities of the three main autotrophic guilds (AMX, AOB and NOB) during operation. The contribution of heterotrophic denitrification to the overall nitrogen turnover was assumed to be negligible (based on specific heterotrophic denitrification tests, Sections 2.6 and 3.6) and is thus not included in the matrix. The matrix A in Eq. 1 refers solely to NH_4^+, NO_2^- and NO_3^-. The actual volumetric activities of the three different guilds (*i.e.* $r_{AMX,cycle}$, $r_{AOB,cycle}$ and $r_{NOB,cycle}$ expressed as $mg_{NH4\text{-}N}\cdot L^{-1}\cdot d^{-1}$, $mg_{NH4\text{-}N}\cdot L^{-1}\cdot d^{-1}$, and $mg_{NO3\text{-}N}\cdot L^{-1}\cdot d^{-1}$ respectively) were obtained by multiplying the process rate with the appropriate stoichiometric coefficient as illustrated here for the case of AOB:

$$r_{AOB,cycle} = \left(-\frac{1}{Y_{AOB}} - i_{N,AOB}\right)\cdot \rho_{AOB}$$

Note: in the text, $r_{AMX,cycle}$ is expressed as sum of both ammonium and nitrite, $mg_{(NH4+NO2)\text{-}N}\cdot L^{-1}\cdot d^{-1}$, to allow for a direct comparison with the maximum anammox activity ($r_{AMX,max}$).

Component	S_{O2}	S_{NH4}	S_{NO2}	S_{NO3}	S_{N2}	X_{AOB}	X_{NOB}	X_{AMX}	**Process rates**
Process	$g_{O2}\cdot m^{-3}$	$g_N\cdot m^{-3}$	$g_N\cdot m^{-3}$	$g_N\cdot m^{-3}$	$g_N\cdot m^{-3}$	$g_{COD}\cdot m^{-3}$	$g_{COD}\cdot m^{-3}$	$g_{COD}\cdot m^{-3}$	$g_{COD}\cdot m^{-3}\cdot d^{-1}$
Growth									
AOB	$-\frac{(3.43-Y_{AOB})}{Y_{AOB}}$	$-\frac{1}{Y_{AOB}}-i_{N,AOB}$	$\frac{1}{Y_{AOB}}$			1			ρ_{AOB}
NOB	$-\frac{(1.14-Y_{NOB})}{Y_{NOB}}$	$-i_{N,NOB}$	$-\frac{1}{Y_{NOB}}$	$\frac{1}{Y_{NOB}}$			1		ρ_{NOB}
AMX		$-\frac{1}{Y_{AMX}}-i_{N,AMX}$	$-\frac{1}{Y_{AMX}}-\frac{1}{1.14}$	$\frac{1}{1.14}$	$\frac{2}{Y_{AMX}}$			1	ρ_{AMX}
Composition Matrix									
gTOD	-1		-3.43	-4.57	-1.71	1	1	1	
gN		1	1	1	1	$i_{N,AOB}$	$i_{N,NOB}$	$i_{N,AMX}$	

Parameters (Hao *et al.* 2002, Hubaux *et al.* 2015)		
Y_{AOB}	0.15	$g_{COD}\cdot g_N^{-1}$
Y_{NOB}	0.041	$g_{COD}\cdot g_N^{-1}$
$i_{N,AOB} = i_{N,NOB}$	0.083	$g_N\cdot g_{COD}^{-1}$
Y_{AMX}	0.159	$g_{COD}\cdot g_N^{-1}$
$i_{N,AMX}$	0.058	$g_N\cdot g_{COD}^{-1}$

Hao, X., J. J. Heijnen, and M. C. M. van Loosdrecht. 2002. Sensitivity analysis of a biofilm model describing a one-stage completely autotrophic nitrogen removal (CANON) process. *Biotechnology and Bioengineering* 77 (3):266-277.

Hubaux, N., G. Wells, and E. Morgenroth. 2015. Impact of coexistence of flocs and biofilm on performance of combined nitritation-anammox granular sludge reactors. *Water Research* 68:127-139.

McIlroy, S.J., Saunders, A.M., Albertsen, M., Nierychlo, M., McIlroy, B., Hansen, A.A., Karst, S.M., Nielsen, J.L. and Nielsen, P.H. 2015 MiDAS: the field guide to the microbes of activated sludge. *Database* 2015, bav062.